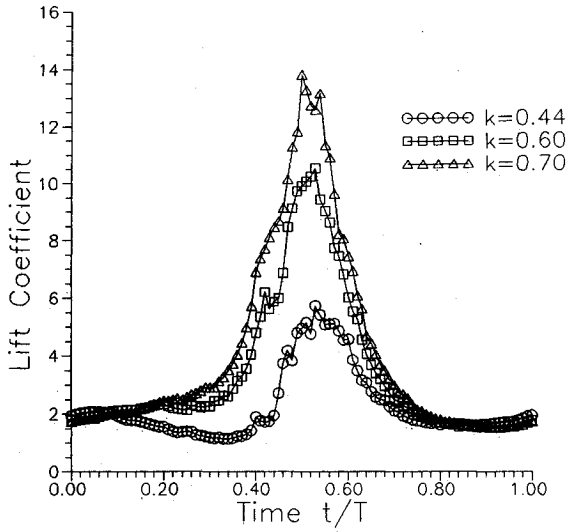

Fig. 3 Variation of phase-averaged lift coefficients for several values of reduced frequency for $R=0.70$.

($t/T=0.25$) and becomes very strong in the middle of the cycle when the freestream velocity is minimum ($t/T=0.5$). With increasing freestream velocity, this vortex is washed away from the wing ($t/T=0.75$).

In Fig. 3, the phase-averaged lift coefficient, defined as

$$C_L(t)=L(t)/\tfrac{1}{2}S\rho U(t)^2$$

is shown as a function of time over a cycle for several values of the reduced frequency at $R=0.70$. Note that all phase-averaged lift curves collapse during the acceleration ($0.8<t/T<1.0$) due to attached flow. This phenomenon has been observed and studied by Shih.[10] For $k=0.70$ (corresponding to the flow visualization photographs), the phase-averaged lift coefficient increases as the size of the separation vortex increases (see Figs. 2). At the middle of the cycle, $t/T=0.5$, the leading-edge separation vortex reaches its climax and is located just above the wing. The size of the vortex is about one chord length. The phase-averaged lift coefficient can be as high as 14 at this moment.

High lift coefficients cannot be explained by acceleration dU/dt (or added mass effect) since the highest lift coefficient during a cycle occurs around $t/T=0.5$, (when the acceleration of the freestream is zero). At this instant, the large separation vortex (Figs. 2) produces highly convex streamlines over the wing and causes a high pressure gradient in the normal direction to the wing surface. Consequently, this greatly increases the suction on the upper wing surface and explains the large lift coefficient at $t/T=0.5$. The value of the lift coefficient at $t/T=0.75$ (when the acceleration is maximum) suggests that the effect of acceleration is small. Moreover, it can be argued that there is no influence of acceleration on time-averaged force (see Fig. 1) since the average value of the acceleration terms is zero (assuming that the load due to acceleration can be written as $a\,dU/dt$, where a is a constant).

Acknowledgments

This work was supported by Air Force Office of Scientific Research Contract F49620-88-C-0061. The authors appreciate the assistance of Hank Lin on the visualization experiment.

References

[1]Carr, L. W., McAlister, K. W., and McCroskey, W. J., "Analysis of the Development of Dynamic Stall Based on Oscillating Airfoil Experiments," NASA TN D-8382, 1977.

[2]Chen, S. H., and Ho, C. M., "Near Wake of an Unsteady Symmetric Airfoil," *Journal of Fluids and Structures*, Vol. 1, 1987, pp. 151-164.

[3]Maresca, C., Favier, D., and Rebont, J., "Experiments on an Airfoil at High Angle of Incidence in Longitudinal Oscillations," *Journal of Fluid Mechanics*, Vol. 92, Pt. 4, 1979, pp. 671-690.

[4]McCroskey, W. J., "Unsteady Airfoils," *Annual Review of Fluid Mechanics*, Vol. 14, 1982, pp. 285-311.

[5]Ericsson, L. E., and Reding, J. P., "Fluid Dynamics of Unsteady Separated Flow. Part II. Lifting Surfaces," *Progress in Aerospace Sciences*, Vol. 24, No. 4, 1987, pp. 249-356.

[6]Lee, M., and Ho, C. M., "Lift Forces of Delta Wings," *Applied Mechanics Review*, Vol. 43, No. 9, 1990, pp. 209-221.

[7]Kruppa, E. W., "A Wind Tunnel Investigation of the Kasper Vortex Concept," AIAA Paper 77-310, AIAA 13th Annual Meeting, Washington, DC, Jan. 1977.

[8]Saffman, P. G., and Sheffield, J. S., "Flow Over a Wing With an Attached Free Vortex," *Studies in Applied Mathematics*, Vol. 57, 1977, pp. 107-117.

[9]Gursul, I., Lin, H., and Ho, C. M., "Vorticity Dynamics of 2-D and 3-D Wings in Unsteady Free Stream," AIAA Paper 91-0010, Jan. 1991.

[10]Shih, C., "Unsteady Aerodynamics of a Stationary Airfoil in a Periodically-Varying Free Stream," Ph.D. Dissertation, Univ. of Sourthern California, Los Angeles, CA, 1988.

Viscous Drag Reduction Using Streamwise-Aligned Riblets

P. Vukoslavčević,* J. M. Wallace,† and J.-L. Balint‡
University of Maryland, College Park, Maryland 20742

I. Introduction

FOR more than a decade, evidence has been accumulating that certain modifications of the geometry of the bounding surface of turbulent shear flows can passively reduce viscous drag. An effective and relatively easy to manufacture modification is a surface of grooves, known as riblets, aligned with the mean flow direction. Although such riblets considerably increase the wetted surface to planform area ratio, they have shown significant net reductions in viscous drag when compared to a similar flow over a flat plate. Their use in the most recent America's Cup regatta caught public attention, and they have been shown to be effective under commercial flight conditions.[1]

A number of investigators have made comparative measurements and computations of the total drag and of the mean and fluctuating velocity fields above riblet and smooth flat-plate surfaces in attempts to document and explain the drag reducing effect of riblets. Walsh and his co-workers,[2-6] using a drag force balance, reported up to 8% drag reduction for triangular riblets of height and span about twice the sublayer thickness, a result later confirmed by the drag balance measurements of Bechert et al.[7] and by pipe flow pressure measurements of Nitschke.[8]

Wallace and Balint[9] compared the streamwise turbulence intensity profiles from various experiments for smooth and riblet surfaces, accounting for the effect on the profiles of Reynolds number variation as documented for smooth surfaces by Purtell et al.[10] With the exception of data of Bacher and Smith,[11] riblets appear to significantly reduce the turbulence intensity over most of the boundary layer, a result that

Received March 19, 1991; revision received July 25, 1991; accepted for publication July 26, 1991.

*Associate Professor; on leave from Veljko Vlahović University, Mašinski, Fakultet, 81000 Titograd, Yugoslavia.

†Professor, Department of Mechanical Engineering.

‡Assistant Research Scientist, Department of Mechanical Engineering.

has been recently confirmed by detailed measurements of Choi.[12] However, none of the measurements compared were able to approach very close to the riblet surface.

Both Bacher and Smith[11] and Hooshmand[13] show little change in the skewness and flatness values of streamwise fluctuations over the riblet surfaces. However, these measurements also were not made very close to the riblet surface. The new results reported in the following sections reveal in detail how much these streamwise fluctuation statistical characteristics are altered by riblets near their bounding surface.

Since changes in turbulent momentum transport must be the cause of the reduced mean velocity gradients at the riblet wall, measurements very near the wall are particularly important. Although Reynolds stress measurements are not reported here, conclusions about the effect of riblets on vertical momentum flux can be inferred from streamwise velocity measurements, as discussed below.

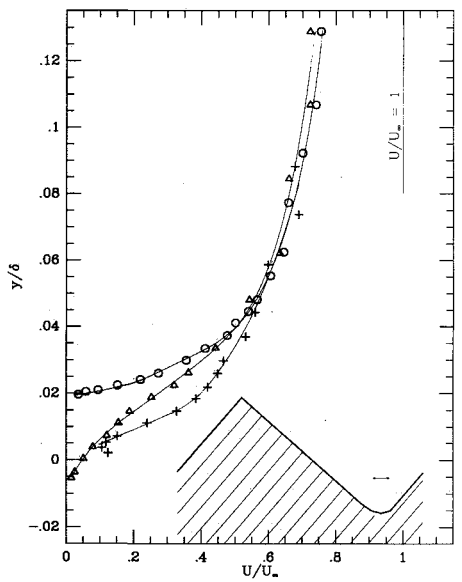

Fig. 1a Mean velocity profiles above the smooth and riblet surfaces normalized with the boundary-layer thickness δ and the freestream velocity U_∞: + smooth surface; Δ riblet valley; O riblet peak. The hot-wire sensor is shown to scale in the sketch above the riblet valley.

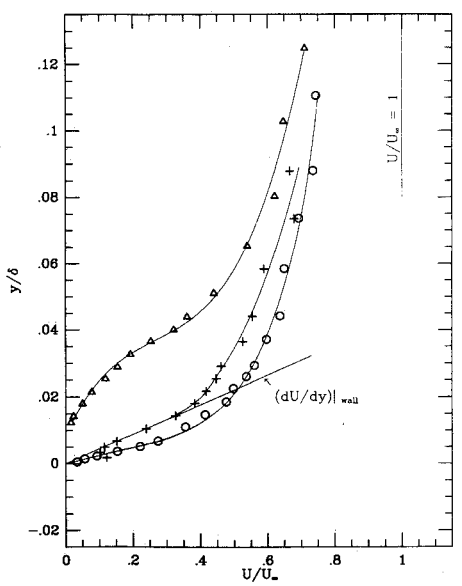

Fig. 1b Data of Fig. 3a with the profiles over the peak and valley shifted vertically so that their surfaces are at the same vertical coordinate origin ($y/\delta = 0$) as the smooth flat plate. Solid straight line represents the mean velocity gradient at the wall determined by choosing u_τ to best fit the logarithmic law.

II. Experimental Facilities and Conditions

The measurements were carried out in a low-speed wind tunnel designed to produce a very thick boundary layer with large scales of turbulence. The boundary layer was tripped at the end of the tunnel contraction by a 5-mm-diam wire and developed on the lower wall of the tunnel over an 8-m fetch. The test surface was the downstream 1 m of this wall where smooth or riblet plates could be interchanged. Both surfaces were made of plastic to reduce heat conduction when the hot wire was brought very close to them. The riblet plate had streamwise aligned triangular grooves of height $h = 5$ mm from peak to valley and span $s = 10$ mm between adjacent peaks. These dimensions, normalized by the viscous length scale $\nu/u_\tau = 0.29$ mm for the comparison smooth-plate flow with the same freestream speed, are $h^+ = 17.5$ and $s^+ = 35$ (or $h/\delta = 0.037$ and $s/\delta = 0.074$), respectively. Here, ν is the kinematic viscosity, u_τ the friction velocity, and δ the boundary-layer thickness. It was not possible to estimate very accurately the span averaged viscous length scale for the riblet plate flow because the span averaged value of u_τ is difficult to estimate. Based on the data that follow, it appears to have been larger than that for the smooth plate, bringing these riblets within the net drag reducing range. At the upstream end of the riblet test plate, the peaks were aligned flush with the tunnel wall. All measurements were made 15 cm upstream of the downstream end of the test plates. To create the thickest developed boundary layer possible in this wind tunnel, which would allow us to use the largest riblets still within the drag reducing range, the tunnel was operated at nearly its lowest stationary speed of 1.23-m/s freestream velocity. This produced a 13.55-cm-thick boundary layer at the measurement location and provided a momentum thickness Reynolds number of $R_\theta \approx 10^3$. That the flow was fully turbulent is evident from the mean and turbulent fluctuation moment profiles for the smooth-plate flow.

The single tungsten hot-wire sensor used for the measurements was 0.5 mm long and 2.5 μ in diameter supported by thin nickel plated tungsten prongs. The probe was fabricated in our laboratory by microwelding the sensor to the prongs followed by briefly nickel plating the sensor and the tips of the prongs to make the probe robust. This allowed us to actually touch the sensor to the peak of the riblet and to the smooth plate surface in order to locate the reference vertical position of the measurements. A sketch showing the probe to scale, positioned within the riblet valley, is shown in Fig. 1a.

To make the measurements as close to the surface as possible while minimizing wall proximity errors, the hot wire was operated at the very low resistance overheat ratio of 1.10. This necessitated careful correction of the sensitivity of the probe's measured output voltages to ambient temperature changes in the flow that occurred during the course of the measurements. With the probe in the calibration position at the center of the tunnel in the freestream, the voltage of the constant temperature anemometer was measured for a range of mean speeds chosen to match those in the near wall layer as the temperature of the flow slowly changed over the temperature range encountered during the boundary-layer measurements. This nearly linear variation was subsequently used to correct all of the instantaneous boundary-layer data to an arbitrary reference temperature. To minimize this correction, the open return tunnel was operated long enough for the temperature in the room to reach a nearly equilibrium state before the boundary-layer measurements began. For all of the data reported herein, the temperature never varied more than 0.2°C.

The anemometer circuits used were constructed after the design of Kaplan[14] and had a flat frequency response up to about 5000 Hz at this tunnel speed. The instantaneous velocity and temperature data were digitized at a rate of 1000 Hz for sample lengths of 30 s.

The probe was calibrated in the freestream over the range of speeds to be encountered in the boundary layer just before and just after each vertical profile was taken. These data were fitted to King's law, $E^2 = A + B(U)^{0.5}$. It was necessary to use

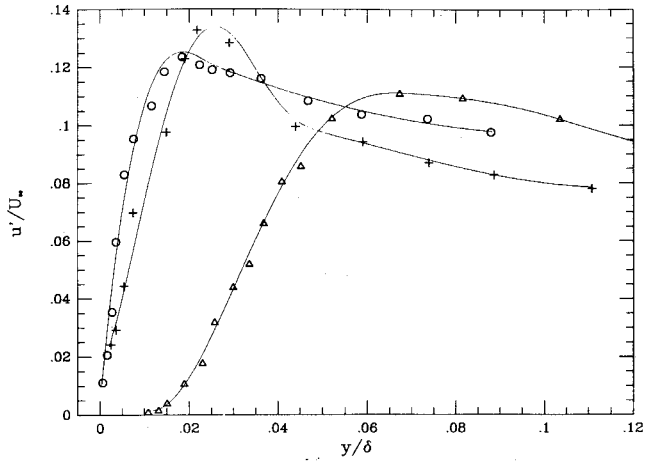

Fig. 2 Turbulence intensity profiles of the streamwise velocity fluctuations above the smooth and riblet surfaces; $y/\delta = 0$ is located as in Fig. 1b. Symbols as in Fig. 1a.

three separate sets of values of the constants A and B for three overlapping segments of the calibration data in order to get the best linear regression calibration fit over the entire range. On completion of the first calibration for each profile, the probe was moved close to the surface by the laboratory computer and positioned, while viewing the sensor with a stereoscopic microscope, so that the hot-wire sensor just touched the peak of the riblet surface or the smooth-plate surface, depending on which plate was in the tunnel. This position was then the reference position of the probe with respect to the surface. The probe was subsequently raised 0.1 mm and the measurements commenced. After the probe had been moved vertically to all of the measurement locations for a given profile, it was recalibrated.

III. Results

A. Mean Velocity Profiles

For comparison purposes and to test the accuracy of the measurements using this low overheat ratio, data were obtained over the smooth surface. Figure 1a shows the smooth-plate mean velocity profile normalized with the boundary-layer thickness δ and the freestream velocity U_∞ and compared to the two velocity profiles over the riblet surface in the planes of symmetry above the peak and valley. In this figure, the origin of the vertical coordinate for the profiles, $y/\delta = 0$, has been located at the midlevel between the riblet peak and the valley. The $y/\delta = 0$ position for the surface of the smooth plate is made to coincide with this location in this figure for comparison. If each of the profiles in the figure is extrapolated to zero velocity, each one intersects the surface at each respective location quite well, neglecting the two points closest to the wall of the smooth-plate profile that exhibit wall proximity effects.

The same data are replotted in Fig. 1b, where the profiles over the peak and valley have been shifted vertically so that their surfaces are at the same vertical coordinate origin ($y/\delta = 0$) as the flat plate. Although the profiles farther from the wall naturally do not match as well as in Fig. 1a, this shift allows better comparison of the slopes of the mean velocity gradients at the respective surfaces. These slopes show the variation of the local wall shear stress at the peak and at the valley of the riblet surface compared to the value for the smooth surface. The solid straight line in the figure, which passes through the flat-plate data near the wall, is the mean velocity gradient at the smooth surface determined from the value of $u_\tau = 0.0554$ m/s, which gave the best fit to the well-established profile in the logarithmic region. The ratio $u_\tau/U_\infty = 0.045$, found from this fit, is a quite reasonable value at the low R_θ of this experiment.

The mean velocity gradient, and thus the local shear stress over the riblet peak, is clearly larger than that over the smooth surface; the increase is approximately 85%. It is not possible to estimate accurately the wall velocity gradient for the valley profile, but it appears to almost vanish to zero at the valley surface. These peak and valley profiles, just above and within the grooves, are quite similar in shape to those calculated by Bechert et al.,[15] but do not show the linear variation above the riblets that their calculation assumes.

B. Turbulence Intensities

The rms values of the streamwise velocity fluctuations have been normalized by the freestream velocity and are plotted in Fig. 2 against y/δ. The smooth-plate profile compares very well to that of Purtell et al.[10] at a similar low Reynolds number. It is quite evident that at a fixed distance above the respective surfaces for $y/\delta \leq 0.05$, for example at $y/\delta = 0.02$, the intensity of turbulence dramatically increases spanwise from the valley to the peak. In the valley of the riblet below the midlevel ($y/\delta \leq 0.02$), the streamwise turbulence intensity almost completely vanishes, never exceeding a value of 1% of U_∞. Comparison of the turbulence intensity above the peak for $y/\delta < 0.02$ with that at the same y/δ location above the smooth plate shows a small relative increase over the peak. This latter result is intuitively expected because the riblet surface, which is inclined away from the peak on each side, is less effective in damping the fluctuations.

C. Skewness and Flatness Factors

The third and fourth normalized moments of the streamwise fluctuations, i.e., the skewness and flatness factors, have

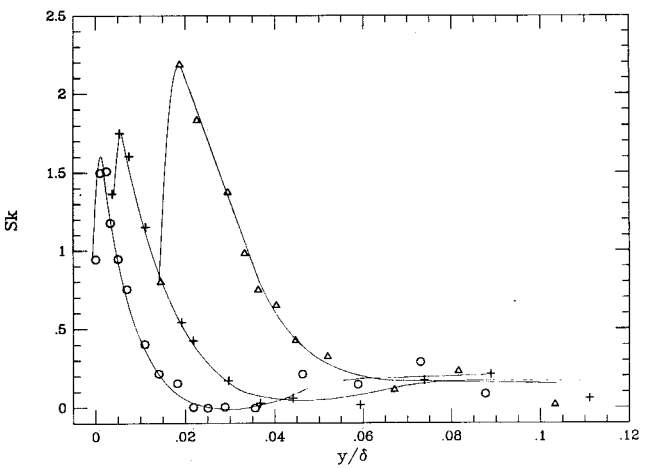

Fig. 3a Skewness factors of the streamwise velocity fluctuations above the smooth and riblet surfaces; $y/\delta = 0$ is located as in Fig. 1b. Symbols as in Fig. 1a.

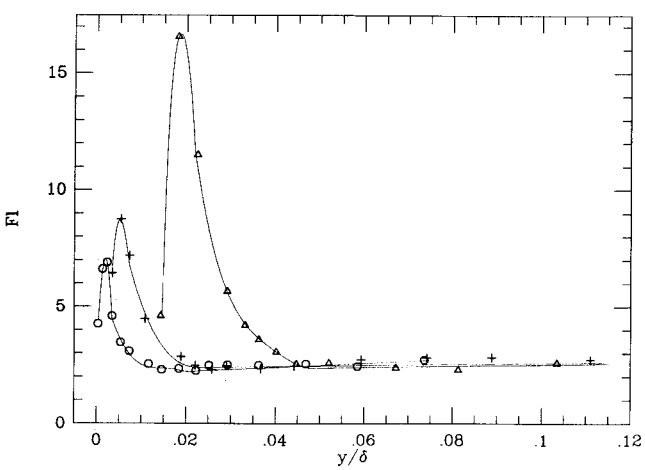

Fig. 3b Flatness factors of the streamwise velocity fluctuations above the smooth and riblet surfaces; $y/\delta = 0$ is located as in Fig. 1b. Symbols as in Fig. 1a.

also been obtained from these data. The three skewness factor profiles are shown in Fig. 3a with the same peak and valley profile shifts as described earlier. The smooth-plate profiles agree well with most data in the literature except that the values for the three locations nearest the wall appear to be somewhat too large because of wall proximity effects (see Alfredsson et al.[16]). At $y/\delta = 0.02$, the skewness factor increases dramatically spanwise from the peak to the valley. The smooth-plate skewness factor values lie between these two extremes. At about $y/\delta \geq 0.04$, the unshifted data collapse approximately to a single curve, indicating that the effects of the riblets on this statistic are confined to the region very close to the surface. This was also seen in Fig. 1a for the mean velocities. The flatness factors above the three surfaces are shown in Fig. 3b and exhibit similar trends. For the unshifted flatness factor profiles, above $y/\delta = 0.04$ all of the data collapse to a single curve.

The extremely large positive skewness and flatness values seen in Figs. 3a and 3b in the riblet valley around the midlevel ($y/\delta \approx 0.02$), when considered together with the small turbulence intensity values in that region in Fig. 2, indicate rare but large amplitude positive streamwise velocity fluctuations due to occasional penetration of fluid from higher in the flow. Below the midlevel, however, the intensity and the skewness and flatness factors in the valley decrease precipitously, showing that the streamwise velocity fluctuations there are almost symmetric and of extremely small magnitude deep within the grooves.

IV. Conclusions

The effects of the riblet surface on the mean and fluctuating streamwise velocity field are clearly exhibited in the $R_\theta \approx 10^3$ boundary-layer data shown earlier. The most dramatic effects are confined to within about 4% of the boundary layer above the riblets measured from the midlevel of the grooves. The local wall shear stress varies greatly in the spanwise direction, from about 85% greater than the smooth-plate value at the riblet peak for flow with the same freestream velocity, to vanishingly small at the riblet valley. The turbulence intensities and skewness and flatness factors of the streamwise velocity fluctuations all indicate that the turbulence nearly vanishes below the midlevel of the grooves. Occasionally, relatively large positive streamwise fluctuations occur in the region between the midlevel and peak of the grooves due to the penetration of the higher velocity fluid from above. However, unlike the vertical momentum transport over the smooth surface, this high momentum fluid rarely gets close to the riblet surface except near the peaks. Thus, the wall stress is lower than the flat-plate value over much of the span. When the resulting spanwise average shear stress is sufficiently lower than that for the smooth plate, more than compensating for the increased wetted surface area of the riblets, net drag reduction occurs.

References

[1]McLean, J. D., George-Falvy, D. N., and Sullivan, P. P., "Flight-Test of Turbulent Skin-Friction Reduction by Riblets," *Turbulent Drag Reduction by Passive Means,* Vol. II, Proceedings of the Royal Aeronautical Society, London, Sept. 1987, pp. 408–424.

[2]Walsh, M. J., and Weinstein, L. M., "Drag and Heat Transfer on Surfaces with Small Longitudinal Fins," AIAA Paper 78-1161, July 1978.

[3]Walsh, M. J., "Drag Characteristics of V-Groove and Transverse Curvature Riblets," *Viscous Drag Reduction,* edited by G. R. Hough, Vol. 72, Progress in Astronautics and Aeronautics, AIAA, New York, 1980, pp. 168–184.

[4]Walsh, M. J., "Turbulent Boundary Layer Drag Reduction Using Riblets," AIAA Paper 82-0169, Jan. 1982.

[5]Walsh, M. J., "Riblets as a Viscous Drag Reduction Technique," *AIAA Journal,* Vol. 21, No. 4, 1983, pp. 485, 486.

[6]Walsh, M. J., and Lindemann, A. M., "Optimization and Application of Riblets for Turbulent Drag Reduction," AIAA Paper 84-0347, Jan. 1984.

[7]Bechert, D. W., Hoppe, G., and Reif, W.-E., "On the Drag Reduction of Shark Skin," AIAA Paper 85-0546, March 1985.

[8]Nitschke, P., "Experimental Investigation of Turbulent Flow in Smooth and Longitudinal Grooved Tubes," NASA TM 77480, May 1984.

[9]Wallace, J. M., and Balint, J.-L., "Viscous Drag Reduction Using Streamwise Aligned Riblets: Survey and New Results," *Turbulence Management and Relaminarization,* edited by H. W. Liepmann and R. Narasimha, Springer-Verlag, Berlin, 1987, pp. 132–147.

[10]Purtell, L. P., Klebanoff, P. S., and Buckley, F. T., "Turbulent Boundary Layer at Low Reynolds Number," *Physics of Fluids,* Vol. 24, No. 5, 1981, pp. 802–811.

[11]Bacher, E. V., and Smith, C. R., "A Combined Visualization-Anemometry Study of the Turbulent Drag Reducing Mechanisms of Triangular Micro Groove Surface Modifications," AIAA Paper 85-0548, March 1985.

[12]Choi, K.-S., "Near-Wall Structure of a Turbulent Boundary Layer with Riblets," *Journal of Fluid Mechanics,* Vol. 208, 1989, pp. 417–458.

[13]Hooshmand, A., "An Experimental Investigation of the Influence of a Drag Reducing, Longitudinally Aligned, Triangular Riblet Surface on the Velocity and Streamwise Vorticity Fields of a Zero-Pressure Gradient Turbulent Boundary Layer," Ph.D. Dissertation, Dept. of Mechanical Engineering, Univ. of Maryland, College Park, MD, 1985.

[14]Weidman, P. D., and Browand, F. K., "Analysis of a Simple Circuit for Constant Temperature Anemometry," *Journal of Physics E,* Vol. 8, No. 7, 1975, pp. 553–560.

[15]Bechert, D. W., Bartenwerfer, M., and Hoppe, G., "Drag Reduction Mechanisms Derived from Shark Skin," *15th Congress, International Council for Aeronautical Sciences,* Paper 86-1.8.3, London, England, UK, Sept. 1986.

[16]Alfredsson, P. H., Johansson, A. V., Haritonidis, J. H., and Eckelmann, H., "The Fluctuating Wall-Shear Stress and the Velocity Field in the Viscous Sublayer," *Physics of Fluids,* Vol. 31, No. 5, 1988, pp. 1026–1033.

Use of Finite Volume Schemes for Transition Simulation

Charles C. Fenno Jr.*
North Carolina State University, Raleigh, North Carolina 27695
Craig L. Streett†
NASA Langley Research Center, Hampton, Virginia 23665
and
H. A. Hassan‡
North Carolina State University, Raleigh, North Carolina 27695

Introduction

THE efficient design of aerospace vehicles requires an understanding and appreciation for the many factors affecting the vehicle's performance. One of the more significant of these factors is the transition of a moving fluid from a smooth, laminar state to one of turbulence. The control of this

Received Oct. 29, 1990; presented as Paper 91-0743 at the AIAA 29th Aerospace Sciences Meeting, Reno, NV, Jan. 7–10, 1991; revision received July 18, 1991; accepted for publication July 18, 1991.

*Research Assistant, Mechanical and Aerospace Engineering. Student Member AIAA.

†Research Scientist, Theoretical Flow Physics Branch, Fluid Dynamics Division. Member AIAA.

‡Professor, Mechanical and Aerospace Engineering. Associate Fellow AIAA.